Annals of Phytomedicine 12(1): 724-735, 2023

DOI: http://dx.doi.org/10.54085/ap.2023.12.1.79

Annals of Phytomedicine: An International Journal
http://www.ukaazpublications.com/publications/index.php

Print ISSN : 2278-9839 Online ISSN : 2393-9885

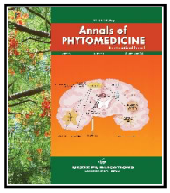

Original Article : Open Access

Phytochemistry and zinc oxide nanoparticles synthesized from ethanolic extract of *Euphorbia serpens* Kunth. and biomedical applications

L. Ravi Kantha Reddy◆ and J. Venkateswara Rao*

Department of Chemistry, Acharya Nagarjuna University, Guntur-522510, Andhra Pradesh,
** Bapatla Engineering College, Affiliated to Acharya Nagarjuna University, Bapatla-522210, Andhra Pradesh, India*

Article Info

Article history
Received 16 April 2023
Revised 4 June 2023
Accepted 5 June 2023
Published Online 30 June-2023

Keywords
Euphorbia serpens Kunth.
Phytochemical analysis
Zinc oxide nanoparticles
Characterization
Antibacterial studies

Abstract

The hydroethanolic extract of *Euphorbia serpens* Kunth. leaves were subjected to a phytochemical analysis using the GC-MS analysis technique in the current study. It was found that the extract is rich in phenolic compounds. Compared to other synthesis methods, producing metal nanoparticles using plant extracts is a simple, dependable, and affordable method. This work looked at the biosynthesis, characterization, and antibacterial activity of ZnONPs made from an extract of *E. serpens*. Nanoparticles were characterized by sophisticated instrumentation for the morphology, elemental composition particles, *etc*. It was found that the typical particle size was 20 nm. Scanning electron micrographs which display damage to the cell walls of the gram-negative bacteria, *Pseudomonas aeruginosa* and the yeast, *Staphylococcus aureus* exhibit the most obvious damage. ZnO exhibits a remarkable rise in absorbance in the UV-V is spectra between 320 and 335 nm. ZnO tensile vibrations at 426 cm^{-1} and 540 cm^{-1} in the FTIR spectrum were quantified. Particle size was determined by SEM analysis to be 30-40 nm. In zeta-size investigations, the particle size was 19 nm, and the particle load was -36 meV. studies on the antibacterial activity of the generated nanoparticles showed that they prevented the growth of *S. aureus* and *P. aeruginosa*. This research demonstrated that ZnONPs could be produced at a low cost and had the potential to be utilized as a carrier system for cutting-edge drug formulations in clinical therapies.

1. Introduction

Nanotechnology is an increasingly important branch of science that aims to develop materials with 1-100 nm dimensions. Nanoparticles find wide use in the health, food, aerospace, pharmaceutical and cosmetic industries. With the development of industrial production at the nanoscale, metal oxides such as silver oxide (AgO), gold oxide (AuO) and other metallic nanoparticles have found a wide market area. Zinc oxide (ZnO) nanoparticles are one of the favourite study subjects of researchers due to their optical and electrical properties (Renganathan *et al.,* 2019). There is no specific area in the literature about how and for what purpose nanoparticles should be used in biological systems. After synthesis, various activity studies are carried out for nanoparticles in many fields. It is known that zinc oxide nanoparticles (ZnONPs) inhibit the growth of various bacterial strains and exert cytotoxic effects against various cancer cell lines (Mishra *et al.,* 2017). ZnONPs are described as excellent drug delivery systems. The US Food and Drug Administration supports the use of ZnONPs (Akbar *et al.,* 2021) with particle sizes larger than 100 nm as a drug delivery system and reports that these particles are biocompatible. ZnO has a broader application potential than other metal oxide nanoparticles because it is relatively inexpensive, biocompatible, and less toxic (Slim *et al.,* 2023). In addition, it has been shown that ZnONPs do not interact with most pharmaceutically active molecules. Stankovic *et al.* (2013) investigated the influence of the morphology and size of ZnO nanoparticles on their antibacterial properties. Using *S. aureus* and *E. coli*, they concluded that a significant difference in the antibacterial efficiency of nanoparticles was observed in both species depending on their shape, with nanospheres being the most efficient, followed by ellipsoids and prism-shaped nanoparticles.

Physical and chemical synthesis have been replaced with green synthesis, which has fewer adverse environmental effects and costs less money. Biological resources, such as plants, bacteria, fungi, and algae, are employed for the green synthesis of nanoparticles (Guan *et al*., 2022). Popularly, the association of medicinal plants with conventional medicines is expected; this intensifies or inhibits the therapeutic effect, consequently interfering with the expected response. In this research study, it was aimed to perform the biosynthesis, characterization and antimicrobial activity of ZnONPs with a simple and easy process with the extract obtained from the green parts of the *E. serpens* plant grown in the Southern Andhra Pradesh, India region. There are very few studies in the literature on the synthesis of nanoparticles from *E. serpens* plant by green chemistry (Ahmad *et al*., 2022). Because the bioactive components (Lalit Kumar *et al*., 2022) in their content facilitate the synthesis of nanoparticles and their harmless effects, studies in this field have increased in recent years (Ahmad *et al*., 2022). In this study, the synthesis of ZnONPs by green chemistry was carried out using *E. serpens* leaf extract. GC-MS studies did photochemistry of the leaf extract, and ZnONPs characterization studies of synthesized

Corresponding author: Mr. L. Ravi Kantha Reddy
Department of Chemistry, Acharya Nagarjuna University, Guntur-522510, Andhra Pradesh, Inida
E-mail: lrkreddy80@gmail.com
Tel.: +91-9848224550

nanoparticles were performed using UV-Vis, FTIR, SEM, zeta potential and EDS analysis. Antibacterial effects of synthesized nanoparticles on *S. aureus* and *P. aeruginosa* were investigated.

2. Materials and Methods

All chemicals and reagents used in the study were purchased from Merck, Sd Fine Chemical with 98-99% purity AR quality. Solutions were prepared with double distilled water (pH:7.02).

2.1 Plant material

E. serpens belongs to the Euphorbiaceae family (Wolf *et al*., 2014) in the plant kingdom; it is a widely distributed species found in tropical and subtropical regions. In Southern India, the species can be found in almost all states in wetlands. The species was observed with flowers and fruits throughout the year and popularly named stonebreaker, white stonebreaker, and combined herb. It was used in kidney stones, bladder, kidney inflammation and as a diuretic. Morphological characters, *viz.,* leaves simple, opposite, petiolate, globous, with entire edge and oblique base (Figure 1). From the literature (Barla Demirkoz *et al.*, 2007), it was identified that it contains phenols, flavonoids, cyanidin's, tannins and saponins in the leaves. Latex contains resins. *E. serpens* differs from all other prostrate species of Euphorbia occurring in Andhra Pradesh, India, in that it is entirely globous and has the appendages of the cyathium petaloid glands, well developed and equal in size.

Figure 1: ***Euphorbia serpens*** **Kunth.**

2.2 Obtaining leaf extract of *E. serpens*

To carry out the extraction tests, 750 g of fresh leaves were manually collected from *E. serpens* located in the rural area of Ongole, Prakasam District. The leaves were collected in October 2018, and then placed to dry in the shade for 15 days. After this drying period, the humidity of the samples was determined using the Dean and Stark apparatus (Pimentel *et al*., 2006). Subsequently, the leaves were crushed in a multiprocessor for 30 sec, homogenized and stored in adequately capped glass vials. The raw material was stored in a domestic refrigerator at 4ºC until use in the extractions. Eighteen grams sample (leaf powder) was added to an Erlenmeyer flask along with 100 ml of solvent (80% water/ethanol solution), according to the procedures described by Redfern *et al*. (2014). The Erlenmeyer flask was covered with cling film. The extraction took place over a period of 24 h, with occasional agitation. Shortly after the end of extraction, the material underwent a vacuum filtration process. Afterwards, the extracts were taken to the oven for complete evaporation of the solvent. In the end, the extracted mass obtained was weighed and used to calculate the yield. The yield of the process was calculated based on Mahyuddin *et al.* (2020) work. Considering the Soxhlet extraction, the yields ranged from 1.53 to 19.74%. According to the literature, solvents significantly influence the extracted compounds. Extractions using non-polar solvents show higher levels of phytoconstituents such as steroids and terpenes, alkaloids and phenols, showing anti-bacterial, anti-inflammatory and antioxidant activity, which would explain the difference between the yields. Confirmation of this fact will be verified after chromatographic analyses of the obtained extracts.

2.3 Characterization by gas chromatography coupled to mass spectrometer (GC-MS)

The analyses were carried out using Shimadzu® QP2010 Ultra GC-MS equipment with a ZB-5HT column (30 m × 0.25 mm × 0.25 m). It was carried out under the following conditions: After 1 min of heating at 60°C, 35 min of heating at 280°C is required. The electron energy was 70 eV, the interface temperature was 280°C, the flow rate of the carrier gas (helium) was 1 ml/min, and the ion source was in scan mode. Injecting 1l of each extract allowed the identification of its constituent constituents *via* comparison with the NIST107 library's mass spectra (Yuan *et al*., 2010).

2.4 Synthesis of ZnO nanoparticles

700 ml of 0.5 M zinc acetate dihydrate (Figure 2B) and 300 ml of hydra ethanolic extract of *E. serpens* were combined. The solutions were continuously stirred at 80°C for 3 h. Following the reaction period, the pH was brought down to roughly 7.0 using sodium hydroxide (0.5 M), which caused precipitates to form. The mixture was centrifuged at 4000 rpm for 20 min and the sediment particles

were then washed with distilled water and 96% ethanol, respectively. The samples were obtained and claimed at 300°C for one hour after being dried at 100°C overnight. Solid particulate material was produced after the synthesis with extract and was kept in hermetic containers until it was characterized and used (Figure 2D). The nomenclature ZnONPs was used in the presentation of the results. Equation 1 can be used to explain the transformation of zinc acetate into zinc oxide nanoparticles in the presence of plant extract.

Figure 2: (A) Ethanolic extract of *E. serpens*, (B) Zinc acetate di hydrate solution, (C) ZnONPs solution and (D) ZnONPs solid particulate material.

2.5 Characterization of nanoparticles

Ultraviolet-visible spectroscopy (UV-Vis): In order to perform a band gap analysis, 50 mg of ZnO nanoparticles were dispersed in 5 ml of water for each sample, creating an aqueous solution, and then subjected to ultrasonic treatment for 180 sec. These samples were analyzed using a Perkin Elmer UV/VIS Lamda 365 spectrophotometer, which scanned a wavelength range of 190 to 700 nm.

FT-IR analysis: About 100 mg of sample was used in the FT-IR analysis of ZnONPs, which was performed using Nicolet IS10 Thermo Scientific FT-IR equipment and a sweep from 500 cm^{-1} to 4000 cm^{-1} using the ATR method (100 scans were performed per reading and three readings were performed).

Scanning electron microscopy (SEM) and electronic dispersive X-ray (EDS) spectroscopic analysis: Cathodic sputtering (JFC-110 ion sputter, JEOL) was used to apply a gold coating to the sample before analysis, which increased the resolution of the resulting image. The samples were photographed at 5 Kev using a scanning electron microscope (JEOL JSM 7600F Tokyo, Japan). Using ImageJ's image processing and analysis software, we counted grains and crystals to understand the size distribution and the average grain and crystal diameter size. The size distribution histograms were generated using Origin Pro 8, a graphics and data analysis program. Measuring at least 180-200 particles or crystals per image from 5 photographs allowed us to calculate the average diameter of each particle or crystal. The same JEOL JSM7600F electron microscope was also used for energy dispersive spectroscopy (EDS) examination of the material's chemical composition across an accelerating voltage range of 0-12 keV.

X-ray diffraction (XRD): Research on X-ray diffraction was performed with a Bruker D2-Phaser X- ray diffractometer. In order to expose the ZnO powders to Cu K^{-1} radiation at a wavelength of 1.5406, they were first pulverized in an agate mortar before being loaded onto a support and set atop a quartz plate. With a two range of 10-70°, a step size of 0.02°, and a count time of 1 s/step, the diffractometer was run at 30 kV and ten mA. The Scherrer equation (Cullity, 1956) was applied to the diffraction patterns obtained from each sample in Jade 6 to estimate the crystallite size.

High-resolution transmission electron microscopy (HRTEM): Ultrasonic dispersion of isopropyl alcohol was used to analyze ZnO samples synthesized with *Hibiscus sabdariffa* flower extracts; a small amount of the suspension was then deposited on a carbon film-coated copper grid and allowed to dry at room temperature before being examined using transmission electron microscopy with a lateral resolution of 0.23 nm and a longitudinal resolution of 0.14 nm, respectively. The micrographs were digitally captured with a Gatan CCD camera (type SC200). The particle sizes were counted, and histograms were generated from TEM images using the ImageJ and Origin Pro 2016 programs.

DLS and zeta potential (æ) analysis: At room temperature (27°C), the hydrodynamic diameter (Dh) was determined by measuring dynamic light scattering (DLS) with a zetasizer nano-ZS from Malvern Instruments (ZEN3500). This experiment used an ultrasonic bath to mix 0.001 grams of the sample with 100 ml of water for 15 sec. Keep in mind that this technique provides an estimate of the mean size of the particles in the medium, even if those particles are too small to be detected individually. The zeta potential of nanoparticle solutions was also measured using the same apparatus at various HCl and NaOH-adjusted pH levels. The effectiveness of 300 ppm solutions of Dh was measured at room temperature.

2.5.1 Determination of the minimum inhibitory concentration (MIC) of the treatment with ZnONP against *P. aeruginosa and S. aureus*in a liquid culture medium

These studies were performed in sterile, 96-well plates with a flat bottom and a cover, using a wide range of doses of both treatments with nanoparticles. Each well, whether it be a treatment or control, received 50 l of a 4X-enriched minimum culture media. The appropriate amounts of sterile distilled water and nanoparticle solution were added using this information to achieve the specified treatment concentrations. When the final volume of 200l was reached

in each well, 1 × 10^8 microorganisms per millilitre (m.o./ml) of the microorganism solution was added. Three wells served as controls without receiving any treatments. As a positive control, *S. aureus* and *P. aeruginosa* were cultured with 5 g/ml of gentamicin. The plates were kept in a 37°C incubator for a whole day. At that concentration, no microorganisms were seen to grow. Therefore, that was taken to be the MIC (Talodthaisong, *et al*., 2021).

2.5.2 Determination of MIC of ZnONP against *P. aeruginosa* and *S. aureus* in solid culture medium:

An enriched minimal culture medium solidified with agarose was used for these tests. The treatments, previously adjusted to the desired concentrations, were added and homogenized to the media before solidification. Negative controls were prepared in the absence of treatments. All Petri-dishes were allowed to incubate at 37°C for 24 h to check their sterility. 200 µl of bacterial solution with a concentration of 1000 CFU/ml was placed, equivalent to 200 CFU, on each agar plate. After incubation at 37°C for 24 h, the CFUs of all the plates were counted and compared with the controls.

3. Results

3.1 GC-MS analysis

Through GC/MS analysis, the qualitative and quantitative composition of the leaf extracts of *E. serpens* was determined using the Soxhlet extraction method results were given (Figure 3 and Table 1). More than 20 significant compounds were identified.

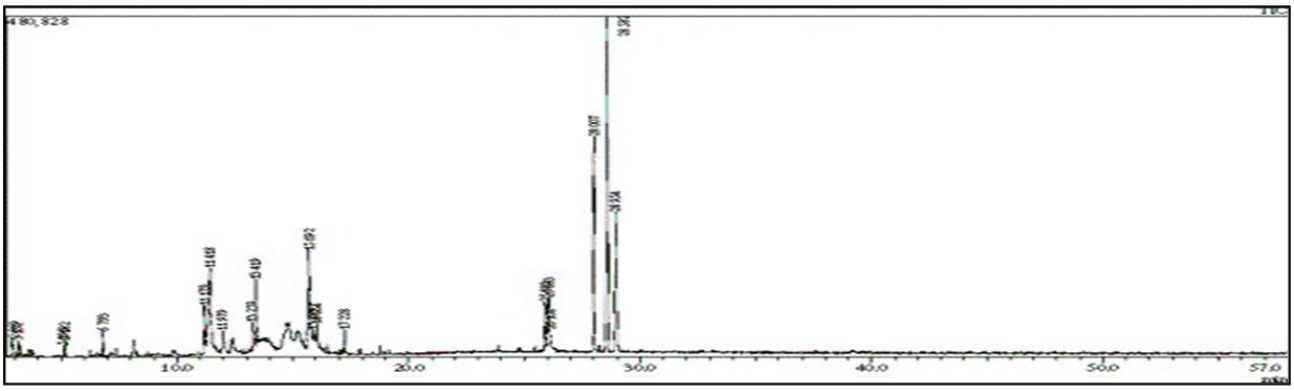

Figure 3: GC-MS of the hydroethanolic extract from the leaves of *E. serpens* obtained by the hot extraction method using Soxhlet.

Table 1: Chemical composition of the crude hydroethanolic extract from the leaves of *E. serpens* obtained by the hot extraction method using Soxhlet

Peak No.	Compound	R.T.	Área
1	Hotrienol	2.87	0.72
2	3,3-Dimethoxy-2-butanone	3.14	0.76
3	2H-Pyran-2,6(3H)-dione	5.1	0.49
4	Oxalic acid, isobutyl pentyl ester	5.19	0.7
5	Hexadecanoic acid, ethyl ester	6.8	0.87
6	1,2,3- benzenetriol	11.19	4.54
7	1,3-Propanediol, 2-(hydroxymethyl)-2-nitro-	11.43	12.44
8	phytol	11.99	1.89
9	Eicosanoic acid	13.27	2.52
10	Hentriacontane	13.43	3.02
11	3,5-diterbutio-4-hydroxyanisole	15.71	8.29
12	Octadecanoic acid, ethyl ester	15.9	1.63
13	2,4(1H,3H)-pyrimidinedione, 5-methyl-	16.07	0.66
14	n-decanoic acid	17.25	0.85
15	2(3H)-furanone, 3,4-bis (1,3-benzodioxol-5- ylmethyl) dihydro-, (3R-trans)-	25.91	3.47
16	Octadecanoic acid, ethyl ester	26.06	4.03
17	4-Hexanoylresorcinol	26.13	0.87
18	Longifolene	28.04	15.71
19	2-Hydroxy-5-methylisophthalaldehyde	28.61	26.25
20	Spathulenol	28.98	10.37

The leaf extract has 1,3-Propanediol, 2-(hydroxymethyl)-2-nitro- (12.44%), 3,5-diterbutio-4- hydroxyanisole (8.29%) (phenolic compounds), Longifolene (15.71%) and 2-Hydroxy-5-methylisophthalaldehyde (26.25%) is a phenolic compound (CHO) and Carissanol dimethyl ether (10.37%) as leading molecules.

3.2 Obtaining and characterization of ZnONPs

Figure 4 shows photographs taken during the synthesis process of the ZnONPs. In these photographs, a reddish precipitate can be seen in the process with *E. serpens*, something like that reported in other investigations (Verma *et al.,* 2020). The colour changes in the solutions and precipitate would be associated with the type and chemical composition of the natural extracts. After calcination, the particles acquired a greyish colour, also reported by Al-Shabib *et al.* (2018). Additionally, before adjusting the pH with sodium hydroxide (NaOH), the solution with *E. serpens* had a pH of 6.34 ± 0.01.

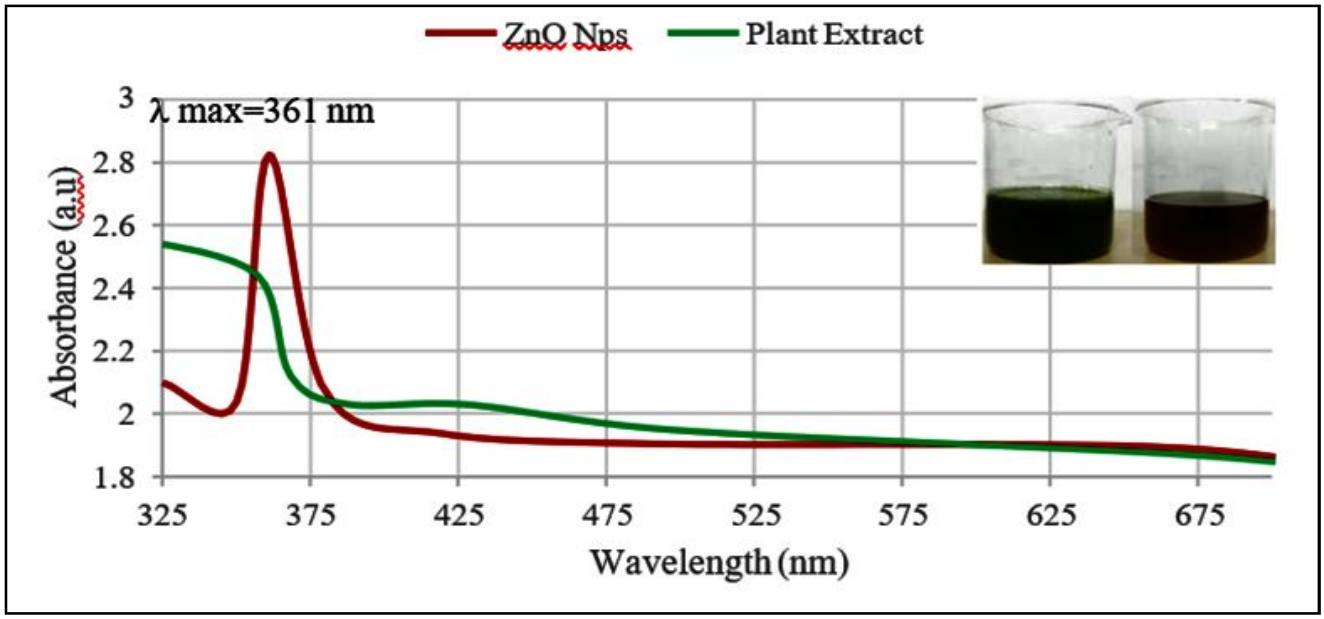

Figure 4: UV-Vis spectra associated with ZnO nanoparticles synthesized with extracts of ethanolic extract of *E. serpens* (change in colour of the solution), while pH (11), plant extract and metal ion ratio = 3:7 and reaction time 180 min.

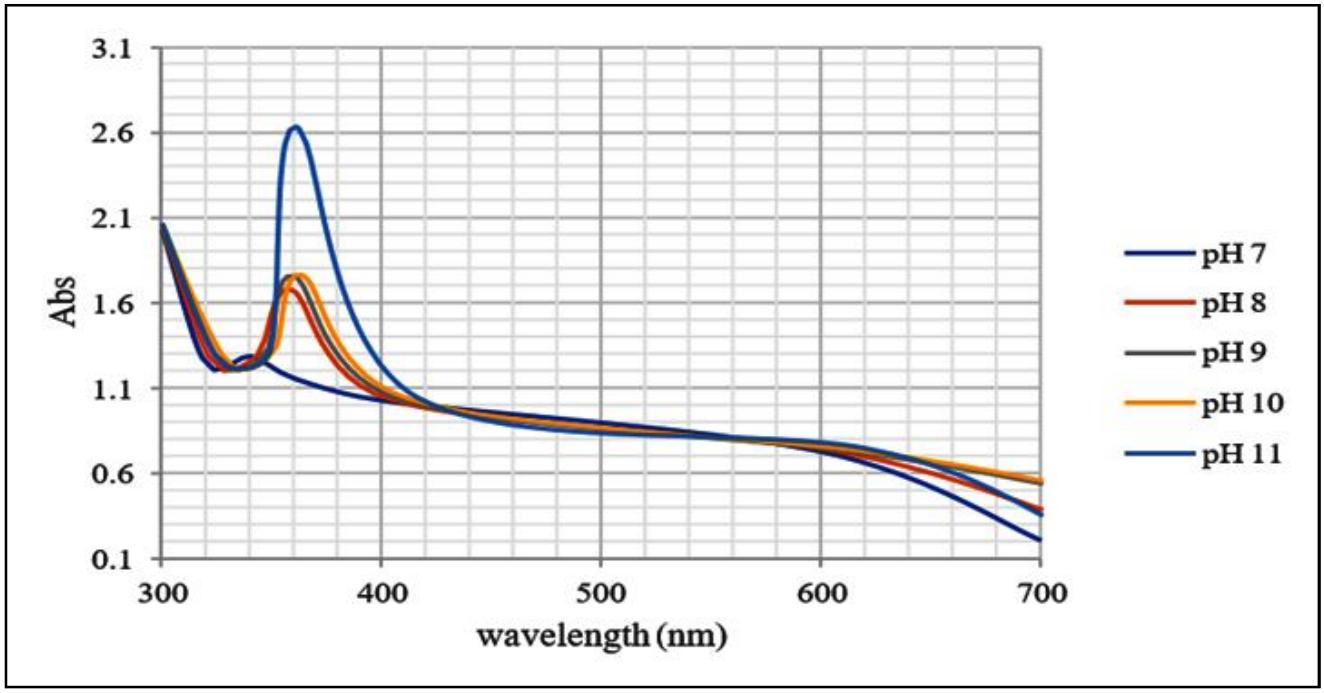

Figure 5: The effect of pH on the green synthesis of ZnONPs.

In Figure 4, it can be seen that in the spectrum of the reactants (*E. serpens* extract only), there is no characteristic absorption; unlike illustration nanoparticles, it can be seen how the spectrum changes after the process to which it was subjected, observing a noticeable change in the Uv-V spectrum. As seen in Figure 5, while the characteristic SPR band of ZnONPs could not be observed clearly at pH 7, it increased with increasing pH and the maximum increase was obtained at pH 11.

An exemplified in Figure 6, when *E. serpan* extract / metal ratio is at least 3:7, the solution turned light cherry colour in the first 15 min and the characteristic surface plasman resonance absorption band (SPR) observed in the 320-370 nm range could clearly be obtained.

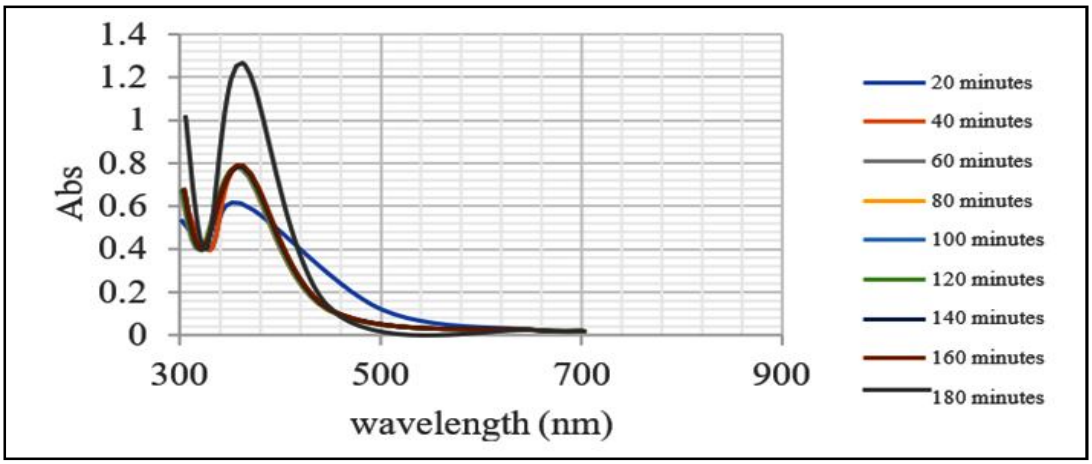

Figure 6: The effect of reaction time on the formation of ZnONPs (*E. serpens* extract/metal concentration ratio (3:7) (20, 40, 60, 80, 100, 120, 180 min for 1-7 curves, respectively).

3.3 X-ray diffraction (XRD)

Figure 7 shows the X-ray diffraction carried out on the sample synthesized in water, ZnO. Eleven planes corresponding to ZnO were observed whose order of height of the intensities between the three prominent peaks did not correspond to the diffraction pattern of the reference card. The plane that diffracted at the highest intensity corresponds to the peak (0 0 2), the second was the plane (1 0 1), and the third most intense peak corresponds to the plane (1 0 0) in Figure 7. The order of intensities on the crystallographic card for ZnO should be the plane of most incredible intensity (1 0 1); the second most intense is (1 0 0), and the third most intense peak corresponds to (0 0 2). Only these three peaks are discussed because they correspond to the characteristic planes of ZnO (Jose *et al*., 2021). 2- theta degree values for 11 peaks in the image identified at 31.88°; 34.55°; 36.40°; 47.74°; 56.82°; 63.13°; 66.65°; 68.24°; 69.37°; 72.90° and 77.28°. Additionally, the ZnO(p) sample showed additional peaks to ZnO that is related to the presence of Mg from the chlorophyll of the infusion used as a reducer during the ZnO biosynthesis process (El-Hawary *et al*., 2021).

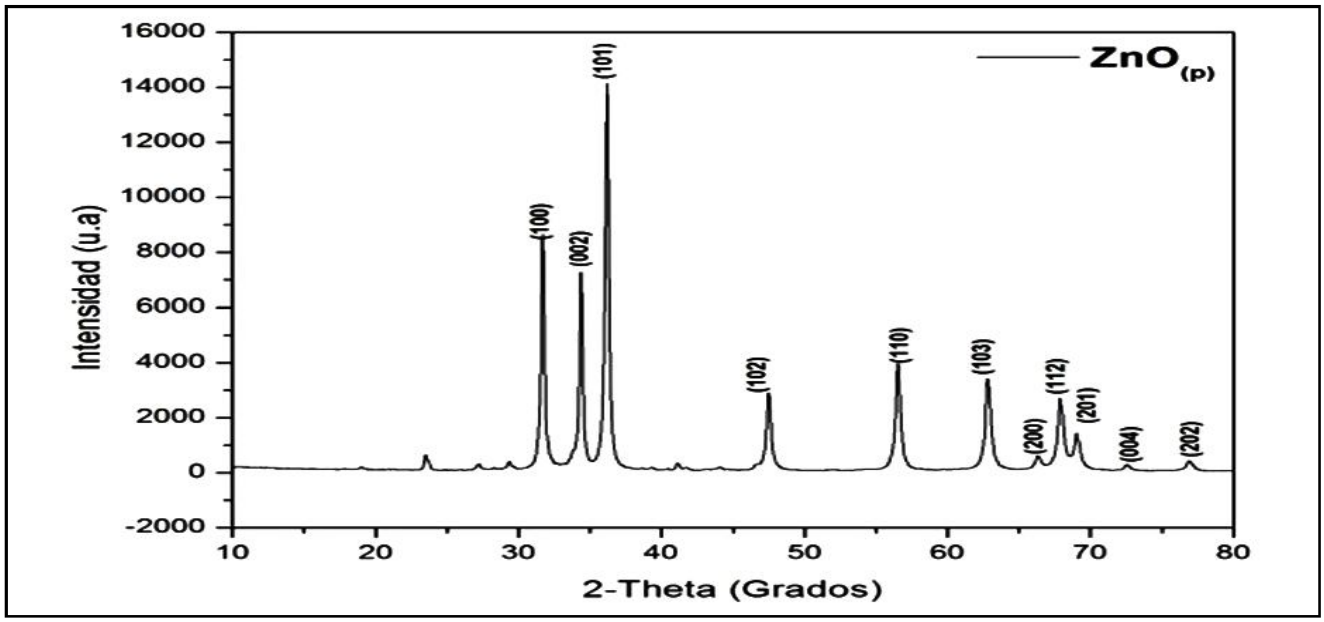

Figure 7: X-ray diffraction spectrum of ZnONPs synthesized from *E. serpens* extract.

3.4 SEM-EDS characterization of nanoparticles

A topographic analysis was carried out by scanning electron microscopy to determine the morphology and size of the ZnO nanoparticles obtained by green synthesis (Saraswathi *et al*., 2020). Figures 8 show the SEM-EDS studies of ZnONPs. In this case, the composition values of each of the elements present in the form of weight percentage were obtained. The three samples show a similar composition; only a slight increase in the amount of potassium ions is observed as the concentration of the extract used in the synthesis increases.

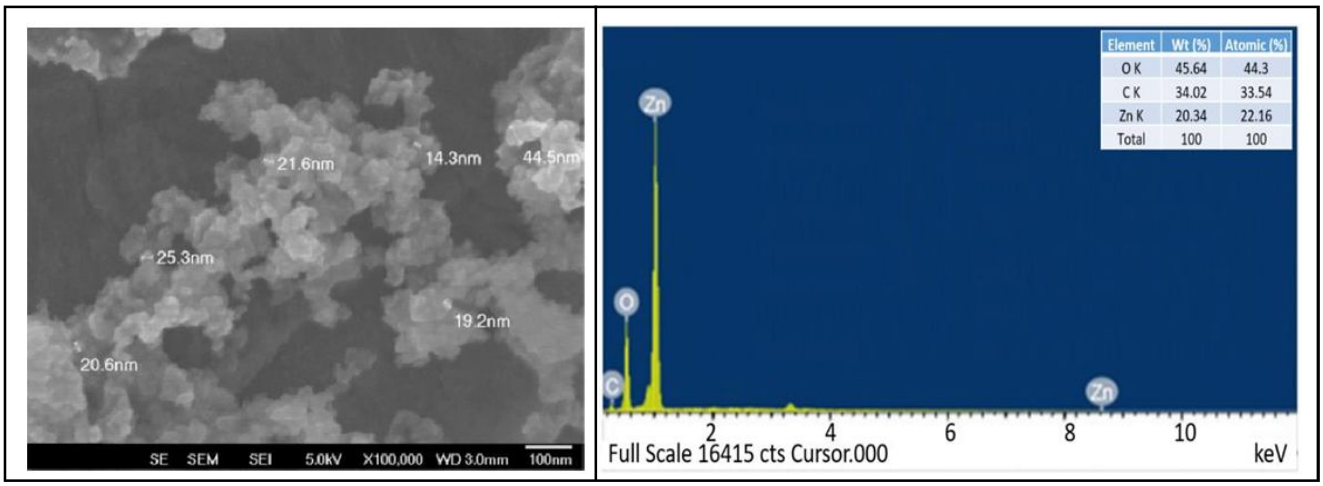

Figure 8: (a) Scanning electron microscopy, in which zinc oxide nanoparticles, with a size range of 14.3 to 44.5 nm. (b) SEM micrographs of ZnONPs and its EDS study.

Zinc was confirmed by EDS spectra, which showed three peaks between 1 and 10 keV, the strongest of which was at one keV (Figure 8b). Since the stoichiometric ratio of oxygen to zinc is 60:30, this means there are no impurity peaks in the sample. As a capping agent for manufactured nanoparticles, stabilizing compounds from the plant extract could explain the spectra's carbon content. Multiple studies have discovered that Zn peaks in the same place on EDS spectra.

3.5 Transmission electron microscopy (TEM) and SAED analysis

Figure 9 shows the transmission electron microscopy (TEM) characterization results of the sample of the ZnO nanoparticles synthesized using plant extract. For the size of ZnO nanoparticles, more than 250 nanoparticles were analyzed using image J, showing the size distribution found for each sample. In Figure 8, the micrograph of ZnO can be seen, in which irregular shapes with minimal tendency to form semi-circles (ovoid) can be distinguished and with the study of size distribution nanoparticles ranging from 20 to 40 nm.

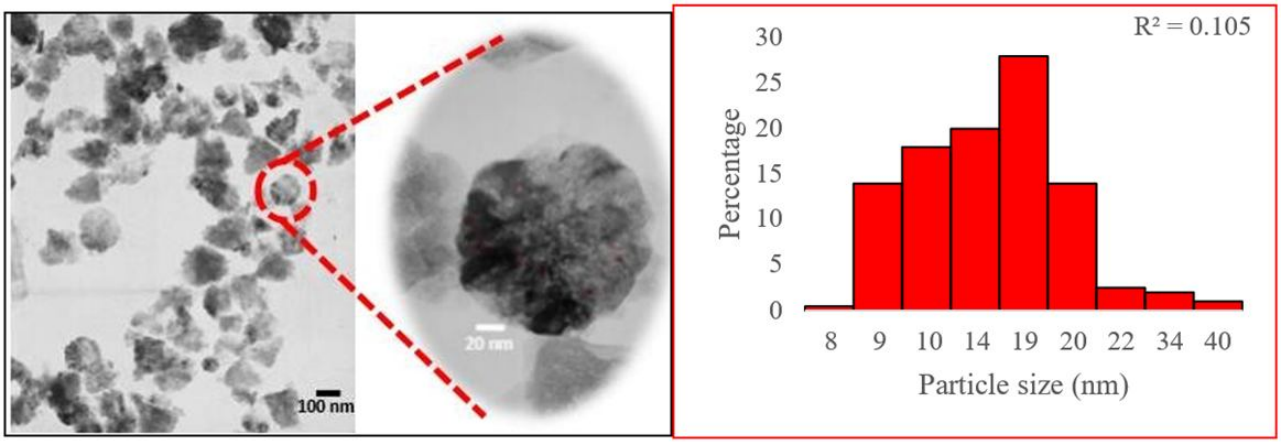

Figure 9: TEM image and size distribution of ZnO nanoparticles.

The HRTEM micrographs are shown in Figure 9, where the effect on the morphology and sizes of the nanoparticles produced by the concentration of extract used in the synthesis (Gungure *et al*., 2021). In addition, the (101) plane is clearly observed for the three samples with an interplanar space of 0.24 nm, directly associated with ZnO's hexagonal crystal system, proving that we have ZnO. The SAED patterns are shown in the boxes of Figure 10, which were indexed according to the hexagonal structure (P63m), JCPDS card number 36-1451, where diffraction rings 1, 2, 3 and 4, corresponding to planes (100), (101), (102) and (101), respectively.

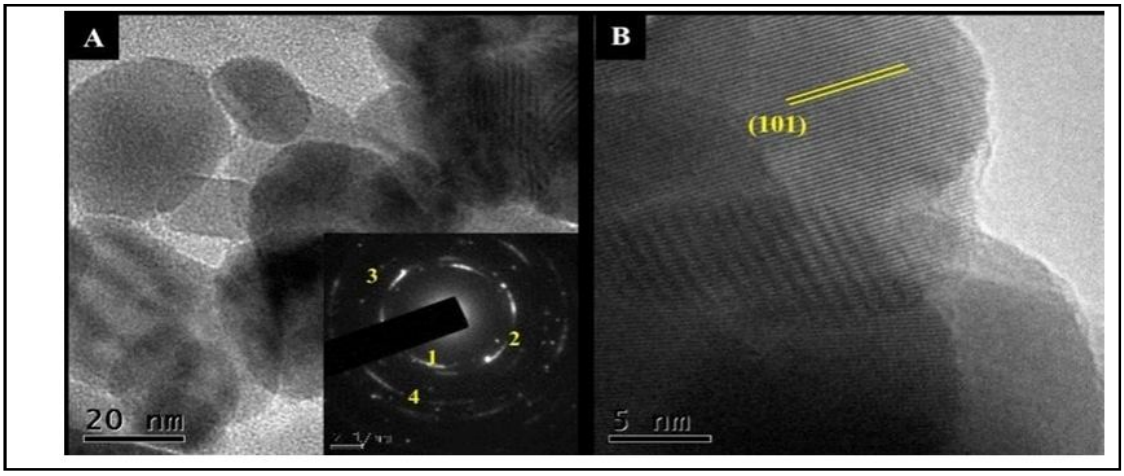

Figure 10: Morphology of ZnO nanoparticles through HRTEM. Show the electron diffraction pattern of ZnO.

3.6 Dynamic light scattering (DLS) analysis

Previously prepared stocks with a concentration of 1 g/l were used to prepare the samples with ZnO nanoparticles. DLS measurements of the ZnO nanoparticle size distribution are shown in Figure 11. The particles have an average size of 2R = 3 nm with a relatively narrow polydispersity ÄR = 0.6 nm. The size parameters in nm correspond to the hydrodynamic diameters obtained by DLS (Ding *et al*., 2020). Apart from these results, the different types of distributions regarding size in intensity, number and volume are also obtained using the zetasizer nano (ZS) software; which can provide additional information. Figure 11 shows the size distribution of the ZnO nanoparticles obtained with the DLS nanosized, where 99.9% of the particles have an average diameter of 9 to 18 nm and 0.1% have an average diameter of more than 20 nm without showing that there are large agglomerations of nanoparticles and having a narrow size distribution.

Figure 11 shows the DLS (right side) and the TEM of a sample of ZnONPs (left side) prepared from ethanolic extract of *E. serpens*. The zeta potential determined (Figure 12) with the zeta meter for the synthesized nanoparticles in sample.

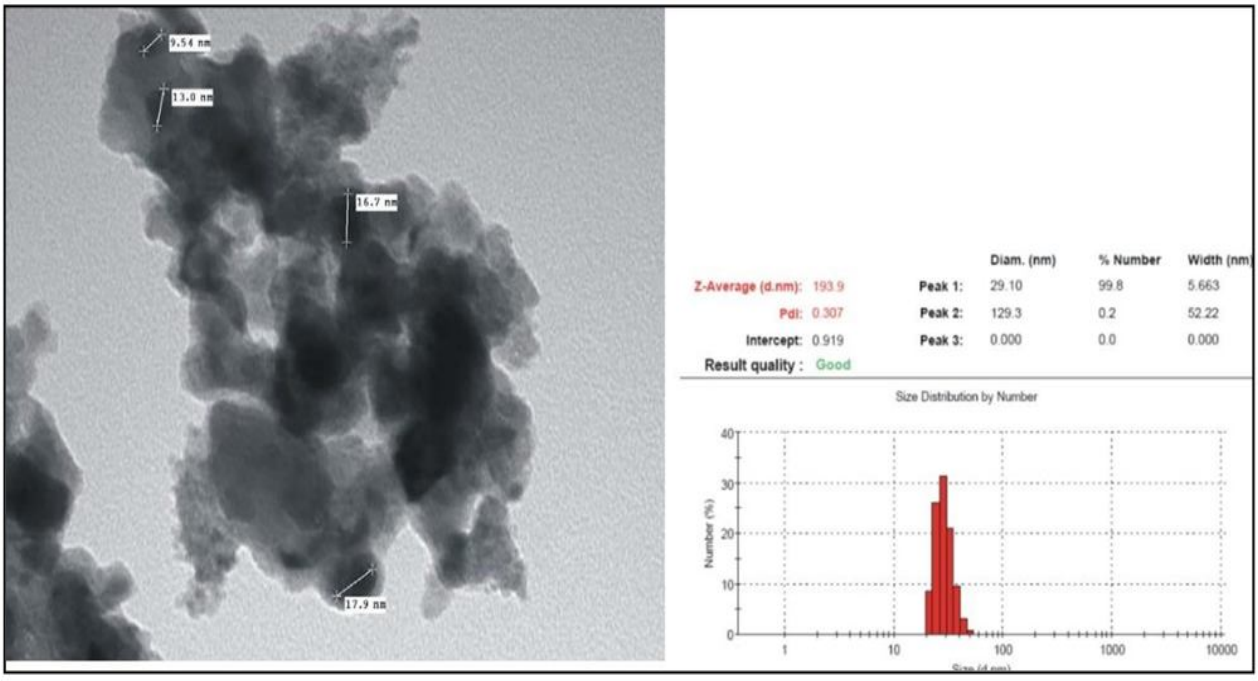

Figure 11: TEM analysis and DSL measurement of ZnO nanoparticles.

A has a value of -36 mV, sufficient to prevent the nanoparticles from agglomerating. Through this technique, the average size of the zinc oxide nanoparticles is determined, as well as their size distribution and their zeta potential. If, the zeta potential is in the range between -30 and + 30 µV, it indicates that the particles can agglomerate. However, if it is less than -30 µV or more significant than +30, the particles will not agglomerate.

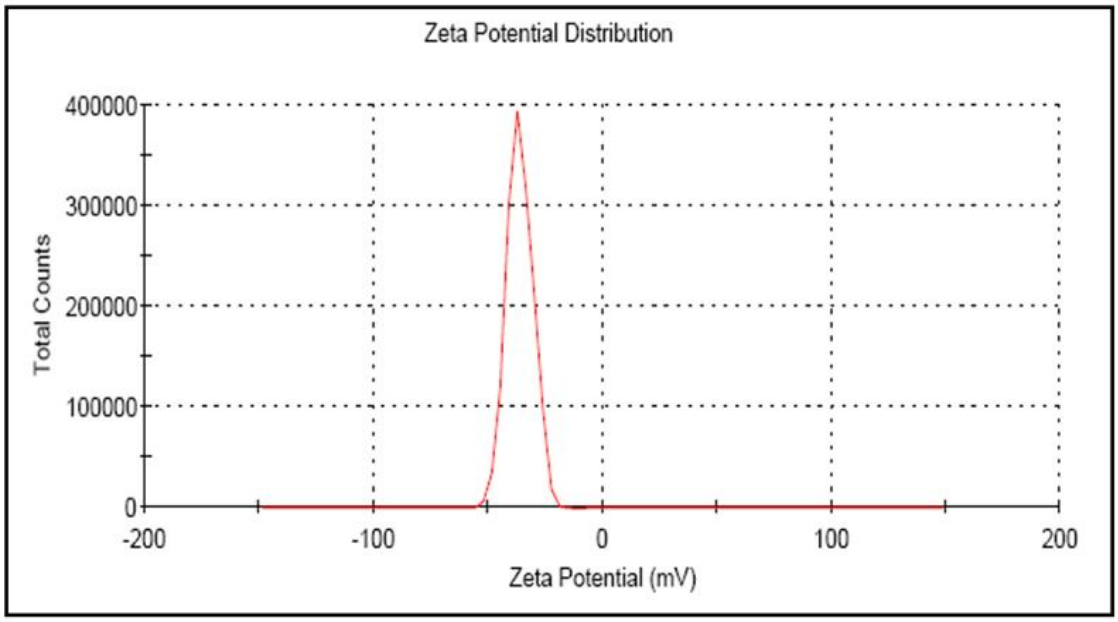

Figure 12: Zeta potential of ZnO nanoparticles synthesized from *E. serpens* extract.

3.7 FT-IR analysis

Figure 12 shows the results obtained from the lyophilized extract of *E. serpens* compared with the spectra of the NPs obtained at 300°C; the characteristic bands associated with the OH elongations are observed at 3283 cm^{-1} of the hydroxyl groups (overlapping with –CH< at approximately 2933 cm^{-1}) and >C=O at 1604 cm^{-1}, in addition at 1396 cm^{-1} a stretching of the carbonyl group. Also, bands related to the stretching and bending of C-O bonds between 1000 and 1100 cm^{-1} are observed. The band at 1604 cm^{-1} is related to the presence of alkene groups corresponding to terpenes, monoterpenes and sesquiterpenes reported in ethanolic extracts of *E. serpens* leaves. Additionally, in the spectrum, a peak located between 400 and 500 cm^{-1} is observed that corresponds to the vibration of the Zn-O bond of the ZnONPs. Ahmad *et al.* (2022) reported FT-IR results of *E. serpens* extracts with different solvents, with the same functional groups reported in this work: hydroxyl, carbonyl, and amines.

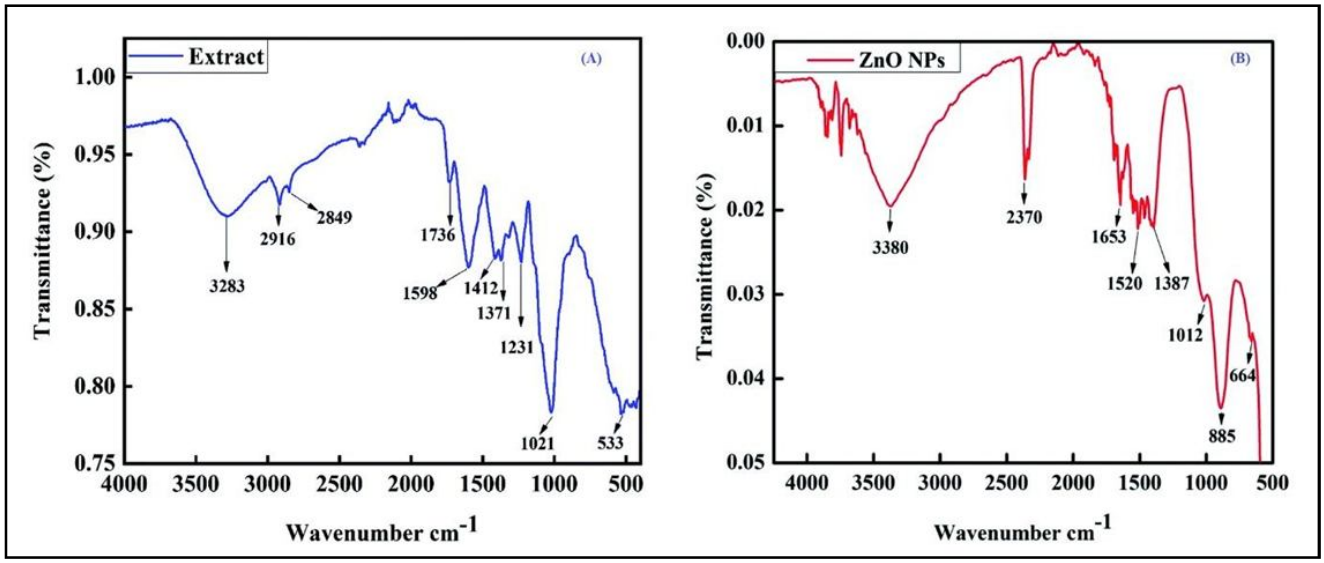

Figure 13: FT-IR spectra and functional groups involved in the synthesis of (b) ZnO nanoparticles obtained at 300°C compared with (a) the extract of *E. serpens*.

Between 1021 and 1012 cm^{-1}, characteristic bands of stretching of the C-N bond are obtained. In general, the previous bands, together with the one that appears at 885 cm^{-1}, indicate the presence and participation of phytochemicals (amines, ketones, alcohols, carboxylic acid, polyols and terpenoids) in the formation of ZnO (Saraswathi *et al.*, 2020).

3.8 Biological studies

In vitro viability assays: Table 2 shows the values determined in assays in 96-well plates with minimal M9 medium. Cytotoxicity of zinc oxide nanoparticles provided by *E. serpens* extract in liquid medium against *S. aureus* ATCC 29213 and *P. aeruginos* ATCC 15442. Zinc oxide nanoparticles presented inhibitory activity against bacteria, especially in a solid medium, since the MICs were much smaller than those observed in a liquid medium.

Table 2: Comparison between the MIC of the nanoparticles in tests carried out in a liquid medium against *S. aureus* and *P. aeruginosa*

Microorganism	MIC of Zn-ONP in an aqueous medium	MIC of Zn-ONP on solid medium
Staphylococcus aureus	MIC 7.0 µg/ml	MIC 1.0 µg/ml
Pseudomonas aeruginosa	MIC 5.5 µg/ml	MIC 2.0 µg/ml

3.8.1 Biofilm analysis by scanning electron microscopy

During the tests with a larger volume of the aqueous medium, it was observed that the bacteria produced a biofilm that captured the NPs, so it was decided to analyze said material to confirm if this biological material contained traces of the metals. Elemental analysis (Figure 14 b) confirmed the presence of ZnO NP captured in a carbon-based compound, presumably organic. Since microorganisms are less exposed to NPs in the presence of the biofilm, the MIC is greater in liquid medium. It is widely known that microbes protect themselves from their surroundings and chemical agents like antibiotics by secreting exopolysaccharides.

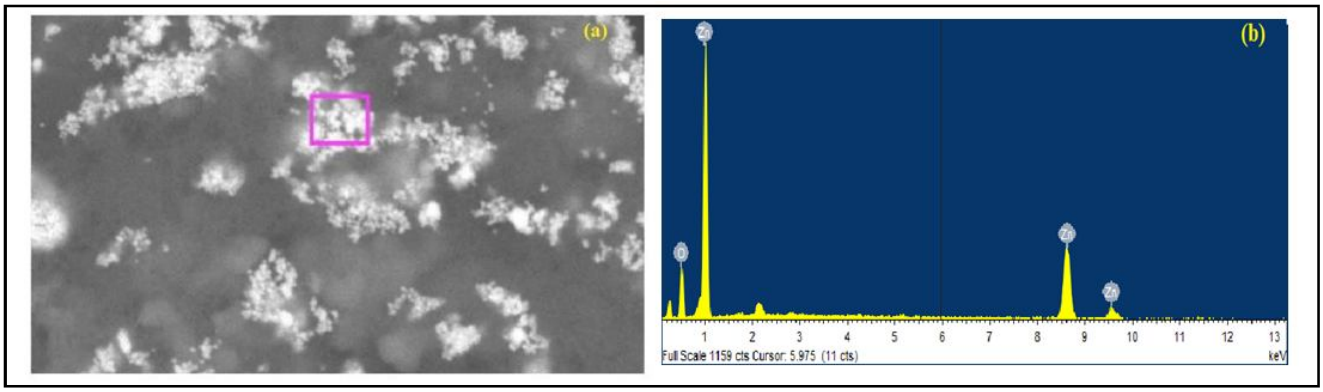

Figure 14: SEM analysis of the exopolysaccharides obtained after exposing *S. aureus* to AgNP. (a) shows the micrograph of the biofilm produced by the bacteria after exposure to treatment. (b) shows the elemental analysis confirming the composition of the material captured in the biofilm.

4. Discussion

Despite the countless studies from antiquity, it is obvious that plants are a natural and limitless source of knowledge. Different techniques are used to extract metallic (MNPs) and non-metallic (NPs) nanoparticles from plants and their extracts. In comparison to other technologies used for these purposes, the synthesis of nanoparticles from plant parts and their extracts is direct and relatively inexpensive. The qualitative and quantitative content of *E. serpens* leaf extracts obtained using the Soxhlet extraction method was evaluated by GC-MS analysis. There were almost 20 major chemicals found. According to Saeed *et al*. (2021), the pH of the synthesis solutions, in addition to influencing the morphology of the nanoparticles, can lead to a variation in the number of ZnO nuclei and the growth of the units, so its adjustment is chosen. In the case of the green synthesis of ZnO nanoparticles, neutral pH has been reported as suitable. Figure 4 shows the UV-Vis spectra of the ZnONPS synthesized with the *E. serpens* alcoholic extracts. As exemplified in Figure 6, when the *E. serpens* extract/metal concentration ratio is at least 3:7, the solution turned light cherry colour in the first 15 min, and the characteristic surface plasmon resonance absorption band (SPR) observed in the 320-370 nm range (depending on the particle size) could clearly be obtained. In addition, the presence of zinc oxide and other elements was confirmed. In the SEM micrographs for the ZnO sample (Figure 8a), hemispherical, dispersed shapes are observed, with few agglomerations and less surface area, while the other samples, with higher extract concentration, show materials that occupy larger areas as the concentration increases.

EDS spectra revealed three peaks, the highest of which was at 1 keV, confirming the presence of zinc (Figure 8b). Since 60:30 is the oxygen-to-zinc stoichiometric ratio, there should be no impurity peaks in the material. The presence of carbon in the spectra may be explained using stabilizing chemicals derived from the plant extract as a capping agent for synthetic nanoparticles. The EDS spectra of Zn have been found to exhibit a consistent peak at the same location.

In the micrograph obtained with the transmission electron microscope (TEM) for powdered sample ZnONPs, it can be seen that the particles have an average diameter of 20 nm, and when performing the dynamic light scattering test, scattering 0.001 grams of the sample in powder in 100 ml of reagent grade acetone and sonicating for 15 sec, an average diameter of 29 nm is obtained, which is consistent with the result of the TEM since in the DLS the hydrodynamic diameter

which is greater than that observed in the TEM, in addition, the size distribution obtained in the DLS indicates that the particles are monodisperse in the range between 20 and 50 nm. Their morphology is spherical, and they are not agglomerated. They are recovered by filtration, washing them three times using ethanol and leaving them to dry in the environment. Green synthesis of ZnO nanoparticles for antimicrobial and vegetative growth applications: A novel approach for advancing efficient, high-quality health care to human wellbeing. On the other hand, considering what Saeed *et al*. (2021) described, the absorption bands between wave numbers 694-660 cm^{-1} could correspond to frequencies in the links Zn-O, suggesting, once again, the synthesis of ZnO. There is no peak in the 6094 to 660 cm^{-1} range in plant extract. Hence, it was confirmed that the Zn-O is absent in plant extract.The presence of the biofilm reduces the exposure of microorganisms to NPs, which correlates with a higher MIC in liquid media. The secretion of exopolysaccharides is a well-known defence mechanism of microorganisms against the environment and chemical agents, including antibiotic.

5. Conclusion

The green synthesis of ZnONPs with a particle size of less than 40 nm was possible, using as a reducing agent the bio compounds of the ethanolic extract of *E. serpens* leaves, making this methodology an economical, easy and environmentally friendly technique.The results of this work show that ZnONPs are toxic to the microorganisms studied. The evidence indicates that the mechanisms for growth inhibition were different for the different microorganisms because their cellular structure is different. Structural damage was confirmed only in *C. albicans and P. aeruginosa*, treated with ZnONPs. In other microorganisms, it is possible that the inhibition mechanism is enzymatic. A defence mechanism by microorganisms against ZnONPs is the formation of biofilms, which was confirmed due to lower inhibitory activity by ZnONPs in the presence of exopolysaccharides.

Conflict of interest

The authors declare no conflicts of interest relevant to this article

References

Ahmad, N.; Fozia; Jabeen, M.; Ul-Haq, Z.; Ahmad, I.; Wahab, A.; Islam, Z.; Ullah, R.; Ahmed,B.; Abdel Daim, M.M.; El-Demerdash, F.M.and Khan, M.M. (2022). Green Fabrication of silver nanoparticles using *Euphorbia serpens* kunth aqueous extract, their characterization, and investigation of its *in vitro* antioxidative, antimicrobial, insecticidal, and cytotoxic activities. Bio. Med. Res Int., **22**:1-11,e5562849. doi:10.1155/2022/5562849.

Akbar, A. and Sadiq, M.M. (2021). Zinc oxide nanomaterials as antimicrobial agents for food applications. In book: "Zinc-Based Nanostructures for Environmental and Agricultural Applications, pp:167-180. doi:10.1016/B978-0-12-822836-4.00012-4.

Al-Shabib, N.; Husain, F.; Hassan, I.; Khan, M.; Ahmed, F.; Qais, F.; Oves,M.; Rahman, M.; Khan, Rais Ahmad; Khan,Md.; Ahmad, I. and Al-Tamimi, J. (2018). Biofabrication of zinc oxide nanoparticle from *Ochradenus baccate* leaves: Broad-spectrum antibiofilm activity, protein binding studies, and *in vivo* toxicity and stress studies. Journal of Nanomaterial. doi:10.1155/2018/8612158.

Barla Demirkoz, A.;Öztürk, M.;Kültür, ª.;Oksüz, and Sevil. (2007). Screening of antioxidant activity of three *Euphorbia* species from Turkey. Fitoterapia, **78**:423-5. doi:10.1016/j.fitote.2007.02.021.

Ding, X.; Lin, K.; Li, Y.; Dang, M.; Jiang, and Lijie. (2020). Synthesis of biocompatible zinc oxide (ZnO) nanoparticles and their neuroprotective effect of 6-OHDA induced neural damage in SH-SY 5Y Cells. Journal of Cluster Science, pp:31. doi:10.1007/s10876-019-01741-2.

El-Hawary, S.; Almaksoud, H.; Saber, F.; Elimam, H.; Sayed,A.; El- Raey, M.M.; Abdelmohsen, U. (2021). Green-synthesized zinc oxide nanoparticles, anti-Alzheimer potential and the metabolic profiling of Sabal black burniana grown in Egypt supported by molecular modelling. RSC Advances. **11**:18009-18025. 10.1039/D1RA01725J.

Guan, Z.; Ying, S.; Ofoegbu, P.; Clubb, P.; Rico, C.; He, F. and Hong, J. (2022). Green synthesis of nanoparticles: Current developments and limitations. Environmental Technology Innovation, **26**:102336. doi:10.1016/j.eti.2022.102336.

Gungure, A.;Jule, L.; Ramaswamy, S.; Priyanka D.and Lalitha,;Gudata,L.; Nagaraj, Nagaprasad.;MekonenAbdisa, B.; Ramaswamy, Krishnaraj. (2021). Green synthesis and characterizations of zinc oxide (ZnO) nanoparticles using aqueous leaf extracts of coffee (*Coffea arabica*) and its application in environmental toxicity reduction. Journal of Nanomaterials, **2**:1-6. doi:10.1155/2021/3413350.

Jose, L.; Arun, R.S.; Sajan.; Aravind and Arun (2021). Adsorption and photocatalytic activity of biosynthesized ZnO nanoparticles using *Aloe vera* leaf extract. Nano Express, **2**(1):1-16. doi:10.1088/2632-959X/abeec6.

Karthick Raja, N.; Selvaraj,; Shyamsundar, D.; Prabanch, M.M.; Arvind, B. and Avinash, G.P. (2021). Inhibitory potential of molecular mechanism of pathogenesis with special reference to biofilm inhibition by chemogenic zinc oxide nanoparticles. Letters in Applied Nano Bioscience, **10**:1862-1870. doi:10.33263/LIANBS101.18621870.

Kumar, S.; Nandha Kumar, E.; Palanisamy, A.; Priya; Das, Soni.; Vimalan, M. and Potheher, I. (2017). Synthesis, antibacterial, antiarthritic, antioxidant and *in vitro* cytotoxicity activities of ZnO nanoparticles using leaf extract of *Tectona grandis* (L.). New J. Chem., pp:41. doi:10.1039/C7NJ02664A.

Lalit Kumar, Laxmi Narayan, S.; Lakshmi Kant and Ramesh Kumar. D. (2022). *In vitro* antibacterial activity of leaves extract of *Eucalyptus globulus* Labill. and *Tamarindus indica* L. against *Rhodococcusequi*. Ann. Phytomed., **11**(2):455-462. doi:10.54085/ap.2022.11.2.55.

Mahyuddin, H.; Roshidi, M.M.; Ferdosh, S. and Noh, Abdul. (2020). Antibacterial Activity of compounds from *Azolla pinnata* extracted using Soxhlet and supercritical fluid (SFE) methods. Science Heritage Journal, **4:** 09-12. doi:10.26480/gws.01.2020.09.12.

Mishra, P.; Mishra, H.; Ekielski, A.; Talegaonkar, S. and Vaidya, B. (2017). Zinc oxide nanoparticles: A promising nanomaterial for biomedical applications. Drug Discovery Today, pp:22. doi:10.1016/j.drudis.2017.08.006.

Pimentel, A.; Graças, C.; Salgado,P.; Aguiar, M.; Silva,F.; Morais,D.; Nelson and David. (2006). A convenient method for the determination of moisture in aromatic plants. Química Nova., pp:29. doi:10.1590/S0100-40422006000200031.

Redfern, J.; Kinninmonth, M.; Burdass, D. and Verran, J. (2014). Using Soxhlet ethanol extraction to produce and test plant material (essential oils) for their antimicrobial properties. Journal of Microbiology,; Biology Education, **15**:45-46. doi:10.1128/jmbe.v15i1.656.

Renganathan, S.; Venkatesan, Hariharan.; Prabakaran, K.; Durairaj, M. and Aroulmoji, Vincent. (2019). Nanotechnology in materials and medical sciences. International Journal of Advanced Science and Engineering, pp:5. 1077-1084. 10.29294/IJASE.5.3.2019.1077-1084.

Saeed, S.; Nawaz, S.; Nisar, Aneesa,; Mehmood, T.; Tayyab, M.M.; Nawaz, M.M.; Firyal, S.; Bilal, M.M.; Mohy-ud-Din, A. and Ullah, A. (2021). Practical fabrication of zinc oxide (ZnO) nanoparticles using *Achyranthes aspera* leaf extract and their potent biological activities against bacterial poultry pathogens. Materials Research Express, pp:8. doi:10.1088/2053-1591/abea47.

Saraswathi, U.; Shahid, M.; Govindarajan, M.; Al-Ghanim, K.; Ahmad, Z.; Virk, P.; Almulhim, N.; Subash, M.; Gopinath, K. and Kavitha, C. (2020). Green synthesis of ZnO nanoparticles for antimicrobial and vegetative growth applications: A novel approach for advancing efficient, high-quality health care to human wellbeing. Saudi Journal of Biological Sciences, **28**:doi:10.1016/j.sjbs.2020.12.025.

Slim, S.;Chérif, I.; Ben-Hlima, H.; Khan, M.M.;Rebezov, M.; Thiruvengadam, M.; Sarkar, T.; Shariati, Mohammad Ali,; Lorenzo and Jose M. (2023). Zinc oxide nanoparticles in meat packaging: A systematic review of recent literature. Food Packaging and Shelf-Life, pp:36. doi:101045. 10.1016/j.fpsl.2023.101045.

Stankoviæ, A.; Dimitrijeviæ, S. and Uskokoviæ, D. (2013). "Influence of size scale and morphology on antibacterial properties of ZnO powders hydrothermally synthesized using different surface stabilizing agents", Colloids and Surfaces B: Biointerfaces, **102**:21-28.doi: 10.1016/j.colsurfb.2012.07.033.

Talodthaisong, C.; Placyao, K.; Mongseetong, C.; Boonta, W.; Srichaiyapol, O.; Patramanon, R.; Kayunkid, N and Kulchat, S. (2021). The decoration of ZnO nanoparticles by gamma-aminobutyric acid, curcumin derivative and silver nanoparticles: Synthesis, characterization and antibacterial evaluation. Nanomaterials, **11**:436-442. doi:10.3390/ nano11020442.

Verma, P; Khan, F. and Banerjee, S. (2020). Salvadora persica root extract-mediated fabrication of ZnO nanoparticles and characterization. Inorganic and Nano-Metal Chemistry, **51**:1-7. doi: 10.1080/ 24701556.2020.1793355.

Wolf, M. and Király, Gergely. (2014). *Euphorbia serpens* (Euphorbiaceae) is a new alien species in Hungary. Acta Botanica Hungarica, **56**:260. doi:10.1556/ABot.56.2014.1-2.16.

Yuan, D.; Yi, L.; Zeng, Z and Liang, Y.Z. (2010). Alternative moving window factor analysis (AMWFA) for resolution of embedded peaks in complex GC-MS metabonomics/metabolomics study dataset. Analytical Methods, pp:2. doi: 10.1039/b9ay00322c.

Zeghad, F.; Djilani, S. E.; Djýlaný, A.; Dicko and Abdou Samad. (2016). Antimicrobial and antioxidant activities of three *Euphorbia species*. Turkish Journal of Pharmaceutical Sciences, **13**:22-37. doi: 10.5505/ tjps.2016.29491.

Citation **L. Ravi Kantha Reddy and J. Venkateswara Rao (2023). Phytochemistry and zinc oxide nanoparticles synthesized from ethanolic extract of *Euphorbia serpens* Kunth. and biomedical applications. Ann. Phytomed., 12(1):724-735. http://dx.doi.org/10.54085/ap.2023.12.1.79.**